

## Docking of Hydroxamic Acids into HDAC1 and HDAC8: A Rationalization of Activity Trends and Selectivities

Gabriella Ortore, Francesco Di Colo, and Adriano Martinelli\*

Dipartimento di Scienze Farmaceutiche, Università di Pisa, via Bonanno 6, 56126 Pisa, Italy

Received August 3, 2009

A docking protocol using Gold software was developed to predict the binding disposition of histone deacetylase (HDAC) inhibitors, starting from the X-ray structures of HDAC8. The optimized procedure was subsequently utilized to dock into HDAC8 and into a homology model of HDAC1 nearly 40 compounds that had been tested for their inhibitory activity against the two HDAC isozymes. Evaluation of the best binding poses allowed us to identify the ligand properties and the protein residues important for activity and selectivity. HDACs are important anticancer drug targets, and their study is currently being actively pursued. As such, our results could help design new isozyme-selective HDAC inhibitors. Furthermore, this strategy may also be used for the investigation of other HDACs.

### INTRODUCTION

Post-translational  $\epsilon$ -acetylation of lysine residues has emerged as a central mechanism of transcriptional control; hypoacetylation results in transcriptional repression and hyperacetylation in transcriptional activation.<sup>1–4</sup> Histone lysine acetylation affects various cellular processes including epigenetic, nongenotoxic, and cancerogenesis,<sup>5</sup> although it is not clear whether epigenetic events can start the process of carcinogenesis in the absence of a classical chemical modification of DNA.<sup>6,7</sup>

Nonhistone proteins such as tubulin and p53 have been shown also to undergo reversible lysine acetylation, evidencing a much broader role of acetylation in controlling cellular events.<sup>8,9</sup>

The lysine acetylation state of cellular proteins is controlled by histone acetyl transferases (HATs) and histone deacetylases (HDACs). There are three classes of HDACs. Class I (HDACs 1, 2, 3, and 8) and class II (HDACs 4, 5, 6, 7, 9, and 10) HDACs are zinc dependent, have a conserved catalytic core, but differ in size and domain structure. Class III HDACs are NAD<sup>+</sup> dependent and dissimilar in sequence and mechanism with respect to classes I and II.<sup>10</sup> Zinc-dependent HDACs have been studied as anticancer drug targets. Inhibitors of these enzymes have been shown to induce terminal differentiation of transformed cells in that they probably alter gene expression by influencing the acetylation state of select histone lysines.<sup>11</sup>

Several HDAC inhibitors (HDACIs) are in phase I or II clinical trials:<sup>12</sup> suberoylanilide hydroxamic acid (SAHA),<sup>13</sup> butyrate,<sup>14</sup> 4-(acetylamino)-*N*-(2-aminophenyl) benzamide (CI-994),<sup>15,16</sup> and cyclo[(2*Z*)-2-amino-2-butenoyl-L-valyl-(3*S*,4*E*)-3-hydroxy-7-mercapto-4-heptenoyl-D-valyl-D-cysteiny], cyclic (3→5)-disulfide (FK228).<sup>17</sup> Most HDACIs mimic the aliphatic acetyl-lysine substrate and possess a hydroxamic acid or other zinc binding group (ZBG), which binds to the catalytic zinc ion at the bottom of a narrow

pocket, as seen in the crystal structures of inhibited histone deacetylase-like protein (HDLP),<sup>18</sup> HDAC-like amidohydrolase (HDAH),<sup>19</sup> and human HDAC8,<sup>20,41</sup> HDAC4<sup>21</sup> and HDAC7.<sup>22</sup> In addition to the ZBG, all HDACIs possess a polar ‘cap group’ (CG), which is usually connected to the ZBG by an alkyl<sup>23–25</sup> or aryl<sup>26–28</sup> linker. However, ‘linkerless’ HDACIs have also been investigated in an effort to produce HDAC8-selective inhibitors.<sup>29</sup> Other than that, isozyme-specific HDACIs have thus far been generated by varying the cap group to exploit variability in the HDAC surface among different isozymes.<sup>25,30</sup> Nevertheless, genuinely selective HDACIs remain difficult to find. Screens of extensive HDACI libraries have yielded selective inhibitors of HDACs 1, 6, and 8.<sup>31,32</sup> However, structure-selectivity relationships are still unknown.

HDAC8 is a peculiar isozyme. Recent studies suggest that HDAC8 is primarily found in the cytoplasm and its expression in primary cells is limited to smooth muscle.<sup>33</sup> Interestingly, RNAi ablation of HDAC8 results in a contraction-deficient phenotype.<sup>34</sup> Thus, establishing the substrates of HDAC8 may broaden our knowledge of targets and functions of HDACs. Moreover, a common form of acute myeloid leukemia (AML) arises from a chromosomal translocation creating an abnormal fusion protein, Inv1, which binds HDAC8 and is correlated with aberrant, constitutive genetic repression.<sup>35</sup> Therefore, efforts against AML may benefit from studies focusing on HDAC8-specific inhibitors.

HDAC1 is also an important member of the HDAC family. Its role in regulating cell proliferation is well known, and this isozyme represents a compelling target in the fight against cancer.<sup>36–40</sup> Overexpression of HDAC1 has been observed in certain forms of cancers.<sup>36–40</sup> Thus, HDAC1-selective inhibitors may demonstrate an enhanced clinical efficacy and/or better tolerability compared to unselective HDACIs.

In this paper, several known HDACIs have been docked into the X-ray structure of HDAC8<sup>20</sup> and into a homology-modeled structure of HDAC1. The most important ligand–receptor interactions are discussed, and a comparative

\* Corresponding author phone: ++39-050-2219556; fax: ++39-050-2219605; e-mail: marti@farm.unipi.it.

**Table 1.** Protein and Zinc Binding Site Alignment Using 1T69 as the Reference Complex

X-ray structure code	protein rmsd	ZBG rmsd
1T64	0.54	0.483
1T67	0.36	0.524
1T69	0	0
1W22	0.49	0.568
2V5X	0.47	0.586
3F07	0.50	1.14
3F0R	0.54	0.920

analysis is carried out in order to rationalize activity trends as well as HDAC1/HDAC8 selectivities.

### COMPUTATIONAL METHODS

Fourteen inhibitor–substrate cocrystal structures have been reported for HDAC8.<sup>20,41–43</sup> Among these, 12 structures contain hydroxamic acids. This, along with the predominance of hydroxamic acid-based HDACIs in the literature, prompted us to devise a docking protocol for hydroxamic acids. Four recent structures, which contain the MS-344 ligand in the D101N, D101A, D101E, and D101L variants (3EZP, 3F06, 3EZT, and 3EW8 PDB<sup>44</sup> codes, respectively), present a mutation that is essential for the interaction with the inhibitor.<sup>43</sup> In addition, unfortunately, the HDAC8-CRA three-dimensional structure 1VKG lacks the Asp89-Pro103 sequence, which is part of the binding site.<sup>20</sup> Thus, we used the remaining seven cocrystal structures for further studies. It should be pointed out that some of the crystallographic structures are dimeric, with the inhibitor binding site being at the interface between the two monomeric units. However, it is known through size-exclusion chromatography and light-scattering experiments that HDAC8 is monomeric in solution,<sup>41</sup> both in the presence or in the absence of inhibitor, so we performed all of our computations using one chain only and one ligand in the binding site.

The seven HDAC complexes<sup>20,41–43</sup> were taken from the Protein Data Bank and used in this work as such (see Table 2); among these, 1T64 and 3FOR contain the same ligand. The hydrogen atoms were added by means of Maestro 7.5<sup>45</sup> using the all-atom model, and water molecules as well as Ca<sup>2+</sup>, Na<sup>+</sup>, and K<sup>+</sup> ions, which lie out of the binding site, were eliminated. Only one chain of the X-ray structure was retained for further computations, whenever the structure was dimeric.

The flexibility of HDAC8 was evaluated by aligning all X-ray proteins, using 1T69 as the reference structure, and analyzing the root-mean-square deviation (rmsd) of the protein backbone for each structure (see Table 1).

The ligands were extracted from the X-ray complexes or built by means of Maestro<sup>45</sup> and subjected to a Conformational Search (CS) of 1000 steps in a water environment using the MacroModel program.<sup>46</sup> The Monte Carlo algorithm was used with the MMFFs force field. The ligands were then minimized using the Conjugated Gradient method to a convergence value of 0.05 kcal/Å mol using the same force field and parameters as for the CS.

The minimized ligands were docked into the proteins using AUTODOCK 4.0<sup>47</sup> and GOLD 3.2,<sup>48</sup> but the former often did not coordinate the ligands to the zinc, so the GOLD program was used for the computations reported in this paper.

The region of interest in Gold was defined in such a manner that it contains all the residues which stay within 10 Å from the ligand in the X-ray structures. The zinc ion was set as a bipyramidal trigonal geometry atom. The ‘allow early termination’ command was deactivated. The default Gold parameters were used for all remaining variables, and ligands were submitted to 40 Genetic Algorithm runs.

Two of the fitness functions implemented in Gold, GoldScore and ChemScore, were used in combination with the scaffold match constraint (SMC) function. The hydroxamic acid moiety (OCNHOH) of the ligand in the appropriate X-ray structure was used as the scaffold, with an SMC weight, the parameter determining how closely ligand atoms fit onto the scaffold, set to the value 10.0. The best docked pose for each ligand was then used for further studies.

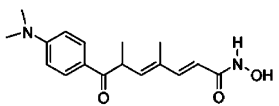
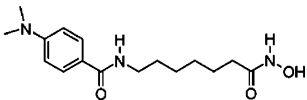
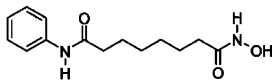
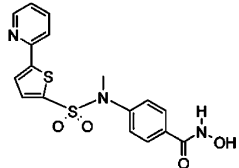
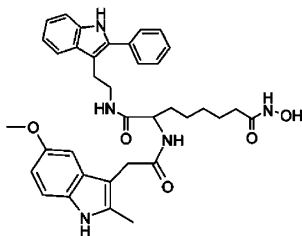
The docking results were visually evaluated using UCSF Chimera.<sup>49</sup> Cross-docking was carried out in order to evaluate the reliability of the Chemscore and Goldscore scoring functions. The HDAC8-inhibitor complex 1T69 was selected as the reference structure, and all other X-ray complexes were aligned to it through the superimposition of the HDAC backbone atoms. The docking reliabilities were then evaluated by calculating the rmsd of the heavy atoms between the above-mentioned experimental reference position and that calculated by Gold for each ligand in each of the seven X-ray complexes. The best docking procedure was used for further studies on the ligands reported in Table 5.

The HDAC1 receptor model was built starting from the 3EW8<sup>20</sup> X-ray structure of HDAC8. This template was returned as the best score hit by the HHSearch program,<sup>50</sup> which uses Hidden Markov Models<sup>51</sup> for template search and shares 41% sequence identity with HDAC1 (Figure 1). Eight PSI-Blast iterations<sup>52</sup> were carried out, with the ‘score secondary structure’ option enabled and using a local alignment mode. The HDAC1 model was obtained from this template through the MODELLER program<sup>53</sup> using the single-template model method and keeping also the MS-344 ligand, which is HDAC6 selective but also binds HDAC1 with an affinity of 0.25 μM. This complex was subjected to 1 ns of molecular dynamics simulation, placing a constraint on the backbone of the whole protein except for the L1 (Gly27-Pro32) and L2 (Pro81-Arg93) loops, which are commonly affected by inhibitor binding in a water environment (using the generalized Born/surface-area model) by means of Macromodel.

The same calculations performed for the inhibitors of Table 5 into HDAC8 were carried out on the final HDAC1 model.

The GOLPE<sup>54</sup> program was used to define a 3D-QSAR model using GRID<sup>55</sup> interaction fields as descriptors and the docking poses as receptor-based alignments for the model. Interaction energies between the selected probes and each molecule were calculated using a grid spacing of 1 Å. The molecular interaction fields (MIF) of C3 (corresponding to a methyl group), N2 (corresponding to neutral flat NH<sub>2</sub>), and O (corresponding to an sp<sup>2</sup> carbonyl oxygen atom) probes were calculated in order to evaluate the lipophilic and H-bond donor/acceptor properties of the ligands and then used for further studies. Variable selection was carried out by zeroing values with absolute values below 0.06 kcal/mol and removing variables with a standard deviation below 0.1. Additionally, variables which either exhibited only two values or had a skewed distribution were also removed.

**Table 2.** Ligands and X-ray Structures Used for Cross-Docking

Ligand structure	Ligand number	X-ray structure code	Reference
 <p>TSA</p> <p>IC50: 490 nM (HDAC8); 1.5 nM (HDAC1)<sup>36-40</sup></p>	1	1T64, 3F0R	19
 <p>MS-344</p> <p>IC50: 249 nM (HDAC1); ND (HDAC1)<sup>39</sup></p>	2	1T67	19
 <p>SAHA</p> <p>IC50: 4000 nM (HDAC8); 119 nM (HDAC1)<sup>36-40</sup></p>	3	1T69	19
 <p>IC50: 175.5 nM (HDAC8); 86 nM (HDAC1)<sup>36-40</sup></p>	4	1W22	35
 <p>IC50: 100 nM (HDAC8); ND (HDAC1)<sup>41</sup></p> <p>APHA</p>	5	2V5X	36
<p>IC50: 3700 nM (HDAC8); 2800 nM (HDAC1)<sup>60</sup></p>	6	3F07	37

## RESULTS AND DISCUSSION

**Cross-Docking.** The docking protocol was first checked by applying a cross-docking approach to the seven HDAC8 complexes with hydroxamic acid-based HDACIs. None of the crystallized inhibitors possesses strong activity (>100 nM) and selectivity for HDAC8 (see Table 2). Analysis of the superposition of the seven crystallographic structures evidence that HDAC8 only undergoes small variations upon changing the ligand, the RMSDs of the protein backbone being about 0.5 Å. The most important variations involve Trp141, in the inner region, as well as Lys33 and Tyr100, which are exposed to the solvent and feel the effects of the L2 loop ligand-induced flexibility. Moreover, little variations also affect Phe152, which, however, seem to be critical for

inhibitor binding. The side chain of the latter residue is flexible enough to accommodate different kinds of linkers and can assume an open conformation which favors binding of CRA-A (5-(4-methyl-benzoylamino)-biphenyl-3,4'-dicarboxylic acid 3-dimethylamide-4'-hydroxamide)<sup>20</sup> and AGE ((2*E*)-*N*-hydroxy-3-[1-methyl-4-(phenylacetyl)-1*H*-pyrrol-2-yl]prop-2-enamide)<sup>43</sup> through the aromatic part of their linkers in the 1VKG and 3F07 structures. Some authors<sup>20</sup> suggest that the Phe152 shift, due to the more sterically demanding aryl hydroxamate CRA-A and the malleability of the HDAC8 active site, permits an enlargement of the subpocket that may be targeted by a new selective inhibitor scaffold. Phe152 shifts are actually not so huge: the heavy-atom RMSDs of this residue in the seven X-ray structures



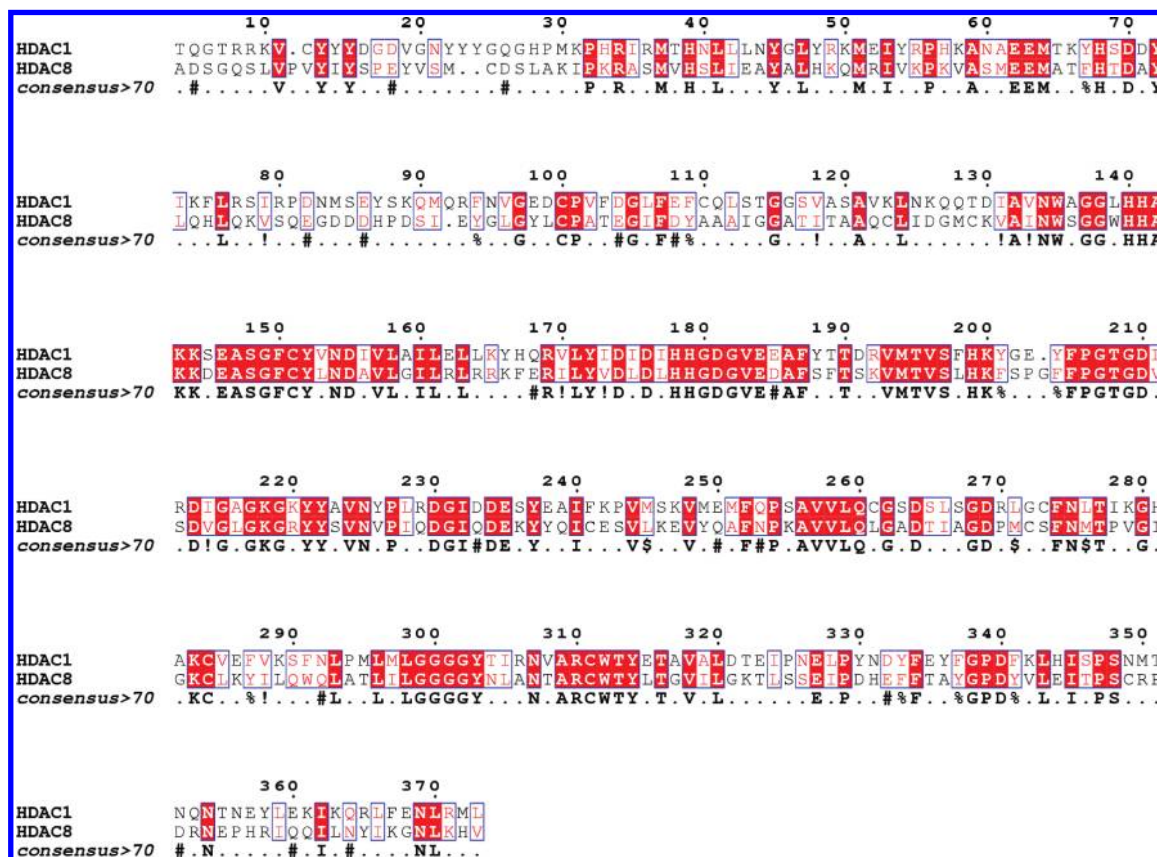


Figure 1. Amino acid sequence alignment of HDAC1 and HDAC8 generated through the PSI-Blast program.

are within a range of 0.1–1.4 Å. However, this residue seems to be determinant, together with Phe208, for the hydrophobic stabilization of the linker in all the diverse isoforms, as has been confirmed through some mutagenesis and molecular dynamics studies on the Phe150 and Phe205 residues of HDAC1.<sup>56</sup> As opposed to the similarity among the residues that make up the binding site channel, different interactions of the surface residues with the CG could favor binding to one of the isoforms over another.<sup>56</sup>

Regarding the ZBG, Table 1 shows that the hydroxamate group adopts similar binding positions in every crystal structure. This allowed us to employ the scaffold match constraint (SMC) function of Gold<sup>57</sup> in our cross-docking computations: this option attempts to place a fragment of every ligand at an exact specified position during the entire docking process. For each ligand docked in turn into the seven available protein crystal structures, the SMC constrained the OCNHOH moiety to overlap to the corresponding atom positions in the proper X-ray crystal structure. Table 2 shows the selected ligands along with the corresponding crystal structures. Each ligand was in turn docked into the seven available protein crystal structures, and the resulting binding disposition was compared to that observed in the X-ray crystal structure of the complex containing the corresponding ligand. For this purpose, the Gold program<sup>48</sup> was employed, after an extensive Conformational Search, and the GoldScore and ChemScore fitness functions were both used.

Tables 3 and 4 display the cross-docking results obtained with ChemScore and GoldScore, respectively. For each protein structure, the RMSDs corresponding to **5** appear always to be significantly higher than those of the other ligands due to the very complex structure of this inhibitor.

Table 3. RMSD Matrix Obtained by the Cross-Docking Study Using the ChemScore Fitness Function<sup>a</sup>

CHEMS	1 2 3 4 5 6						row_av
	1	2	3	4	5	6	
1T64	1,2	3,73	3,5	2,46	7,54	2,97	3,19
1T67	3,07	2,48	2,08	2,41	3,98	2,67	2,83
1T69	1,45	1,6	1,52	0,96	4,89	2,62	2,10
1W22	2,95	3,38	2,38	2,73	4,61	5,77	3,58
2V5X	2,99	2,78	3,26	2,84	3,65	1,44	2,90
3F07	5,05	5,91	1,37	2,48	4,55	1,24	3,71
3F0R	1,32	4,07	3	3,02	7	2,93	3,18
col_av	2,58	3,42	2,44	2,41	5,17	2,81	
self dock av	1,97						

<sup>a</sup> Key: white, RMSD ≤ 2.0 Å; yellow, 2.0 < RMSD ≤ 4.0 Å; red, RMSD > 4.0 Å.

The ChemScore function was able to predict the right binding disposition of the ligands with a rmsd < 4 for about 80% of the cross-docking poses. The self-docking results show a good reproducibility of the experimental data for ligands with such a degree of flexibility with an average rmsd of 1.97 Å. In the self-docking, we also obtained the highest rmsd for the 2V5X complex. The GoldScore fitness function yielded less promising results than those obtained through ChemScore, the 4.0 Å rmsd threshold value being exceeded for 40% of the cross-docking results. The “row-average” rmsd analysis designates structure 1T69 as the most reliable protein for predictive purposes, with a ChemScore average rmsd of

**Table 4.** RMSD Matrix Obtained by the Cross-Docking Study Using the GoldScore Fitness Function<sup>a</sup>

Using the GoldScore Fitness Function								
PROTEINS	GOLDS						row_av	
	1	2	3	4	5	6		
	1T64	0,97	4,03	3,72	2,28	8,42	3,01	3,34
	1T67	2,88	3,04	1,88	2,51	5,32	2,65	2,92
	1T69	0,98	5,98	1,54	4,47	10,16	3,26	3,97
	1W22	3,12	4,88	5,21	7,16	10,36	3,54	5,40
	2V5X	2,77	4,41	3,41	3,28	10,39	6,13	4,82
	3F07	5,31	5,59	5,91	5,23	3,34	3,85	4,99
	3F0R	1,57	4,3	3,18	3,13	7,72	2,82	3,41
	col_av	2,51	4,60	3,55	4,01	7,96	3,61	
self dock av		4,01						

<sup>a</sup> Key: white, RMSD  $\leq$  2.0 Å; yellow,  $2.0 < \text{RMSD} \leq 4.0$  Å; red, RMSD  $> 4.0$  Å.

2.10 Å. In conclusion, we decided to use protein 1T69 and ChemScore for our further docking computations.

**HDAC8.** Since our final goal was to rationalize HDAC1/HDAC8 selectivities, we chose to only carry out docking computations on hydroxamic acids for which the HDAC1/HDAC8 IC<sub>50</sub> ratio was  $<0.1$  or  $>10$ . The selected ligands are reported in Table 5. The first group consists of substituted benzimidazoles and indoles, while a second group comprises some biaryl and phenylthiazolyl compounds. These compounds have been recently published in some patent applications,<sup>26–28</sup> and for some of them the biological activity is expressed only as range of IC<sub>50</sub>  $< 100$  nM or  $>1000$  nM. In these cases, we choose to consider an IC<sub>50</sub> of 100 and 1000 nM, respectively. A third class of compounds encompasses six “linkerless” HDAC8-selective inhibitors<sup>29</sup> whose activity values have been determined through western-blotting instead of the fluorescence-based methods that have been used for the first two groups of ligands. These compounds will be discussed separately because the corresponding biological data are not comparable with those of the other ligands.

Except for the “linkerless” inhibitors, all these ligands have the same general structure, which is made up of the hydroxamic acid zinc binding group (ZBG), an all-aliphatic or partly aromatic linker, as well as a cap group. The latter is supposed to act as a surface-recognizing entity, which can be elaborated upon in order to achieve isozyme selectivity.<sup>25</sup>

As far as the ZBG is concerned, its two oxygen atoms coordinate to the zinc, whose trigonal bipyramidal coordination sphere is completed by Asp178, His180, and Asp267. Such a binding arrangement mimics what is thought to occur at the beginning of the zinc-assisted hydrolysis reaction involving acetylated peptidic substrates. Indeed, in this case the substrate interacts with the zinc ion through its carbonylic oxygen, while the zinc vacant site is filled up by one molecule of water.<sup>20</sup> The hydroxamic acid moiety is involved in a complicated network of hydrogen bonds with His142, His143, Asp178, His180, and Tyr306. This also mimics the above hydrolysis reaction, where His142 and His143 are supposed to hydrogen bond to the water molecule while a third hydrogen bond from Tyr306 polarizes the acetyllysine's carbonyl group.<sup>20</sup> It should be pointed out that each

of the ZBG hydrogen bonds is expected to be stronger than a normal hydrogen bond in that the ZBG is polarized by the zinc ion. Therefore, these hydrogen bonds, along with the ZBG–Zn coordinative interactions, presumably account for most of the ligand binding energy. All these ZBG hydrogen bonds are conserved throughout our set of ligands.

The linker is not a mere spectator. Indeed, it finds itself in a narrow channel with hydrophobic walls, made up by Gly151, Phe152, His180, Phe208, Met274, and Tyr306, and gives rise to lipophilic interactions with these residues. The nonconserved Tyr100, Lys33, Met274, Phe207, and Gly206 residues divide the binding site surface into four different pockets: the first one delimited by Lys33 and Met274, the second by Met274 and Phe207, the third by Gly206 and Asp101, and the smallest by Tyr100 and Lys33 (A, B, C, and D pockets in Figure 2, respectively). The interactions with these hydrophobic walls develop within each of the studied HDAC8–inhibitor complexes, including when the linker is partly aromatic. It seems important to analyze the effect of the linker structure because it plays a role in selectivity. Indeed, the HDAC8/HDAC1 selectivity trend of compounds bearing a short partly aromatic linker (scaffolds **c** and **d**, compounds **16–23**) is very different from that of ligands with a medium-sized linker (scaffolds **a** and **b**, compounds **7–15**) and a long aliphatic linker (scaffolds **e** and **f**, compounds **24–42**). Figure 3 shows the effect of the linker structure on the docking poses: the aromatic short linker of compounds **16–23** favors the interaction of the CG with Phe207 and Met274. On the other hand, the longer linkers of compounds **7–15** lie in the A pocket and the aliphatic chains of compounds **24–42** direct their CGs toward the L2 loop.

Compounds with **a** and **b** scaffolds bearing two quite bulky substituents (R and R'), such as compounds **7**, **9**, and **11** (cyan, gray, and green in Figure 3a, respectively) insert their R moiety into the A region of the surface and the R' group into the C pocket, which has a peculiar backbone conformation in the region of the nonconserved Gly206 residue. Compounds with a comparatively short chain in the R' position place the latter near Asp101: in particular, the hydroxy and methoxyethyl groups of compounds **8**, **10**, **14**, and **15** (cyan, green, orange, and gray in Figure 3b, respectively) engage in hydrogen bonds with this residue, and their R substituent lies in the B pocket, except for the rigid methoxyphenyl moiety of compound **8** which occupies the C pocket. The biological data of these compounds show a micromolar range of activities, without large differences, ranging from a minimum of 0.13  $\mu\text{M}$  for compound **15** to 0.6  $\mu\text{M}$  for **11**. There is no clear evidence for structure–activity relationships, but the docking results seem to suggest that the polar interaction with Asp101 can stabilize the ligands, and a further enhancement of the binding could be due to the van der Waals interactions with the binding site surface in the region of Met274 and Phe207.

Among the compounds with **c** and **d** scaffolds, the docking orientations are essentially the same and presumably strong interactions with the binding site are mirrored by comparatively high activity values. The short aromatic linker of compounds **16–21**, all of which bear very similar CGs, allows the same binding disposition (see Figure 3c) in a pocket due to Gly206, Phe207, and Met274, all nonconserved residues. Such an orientation is presumably well stabilized,

owing to an aromatic stacking interaction involving Phe207. Compound **22** (gray in Figure 3c), the c-scaffolded ligand with the longest CG, can adopt a similar binding mode by establishing an aromatic interaction with Phe207.

Our docking computations yielded very different results for compounds **24–42**. The CGs of these compounds are very far from the nonconserved region around Phe207, point toward the L2 loop, and cannot make effective interactions with any residue. As shown in Figure 3, all the linkers of compounds **24**, **30**, **32**, and **38** have the same binding disposition and interact with Asp101 through their amidic NH. The terminal phenyl group of compounds **24** (orange) and **32** (cyan) adopts slightly different orientations in the two cases due to the different nature of the scaffolds but in both cases points toward the outside of the protein. More complex and bulky CGs can occupy the large space between Tyr100 and Tyr306, such as the amidopyrrolidine of compound **30** (gray), or the free region toward the L2 loop, such as the CG of compound **38** (magenta), which has the same binding disposition as compounds **37**, **39**, and **40**, without any effective interaction with the protein.

Regarding the series **43–48**, only compounds **45**, **47**, and **48** (yellow, blue, and green in Figure 4, respectively) occupy the binding channel, and their ZBG can effectively coordinate

to the zinc. Despite the lack of a linker, their CGs interact with the surface and point toward the B region. Compounds **43**, **44**, and **46** (magenta, cyan, and red in Figure 4, respectively) occupy a nearby internal cavity without coordinating to the zinc, and their CGs cannot reach the surface.

In conclusion, the docking analysis seems to suggest that, in addition to the predominant ZBG interactions, the interactions the CG establishes with the active site surface are essential. No interaction is strong enough to justify the activities of the best inhibitors, yet different interactions appear to have a binding effect. The nature of the linker emerges to be crucial to direct the CG toward a peculiar region of the HDAC8 surface, i.e., the nonconserved lipophilic area designed by Gly206, Phe207, and Met274. All the compounds that strongly interact with this region, such as compounds **16–23**, and also compounds **45**, **47**, and **48**, show the best values of activity.

**HDAC1.** The HDAC1 receptor model was generated using the human HDAC8-MS344 cocrystal structure determined at 1.8 Å resolution (3EW8)<sup>20</sup> as the template. This template shares 41% sequence identity with HDAC1 and covers the sequence of interest from amino acid 4 to 373 (Figure 1).

On the basis of the alignment with the template, the HDAC1 model was built by means of the Modeler pro-

**Table 5.** Ligands Docked into HDAC1 and HDAC8

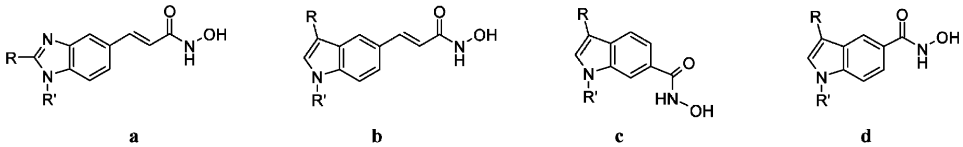
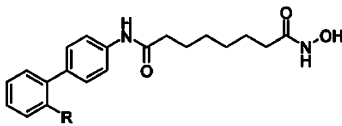
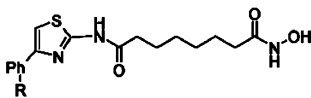
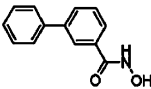
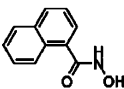
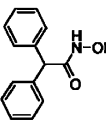
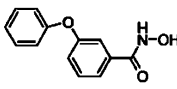
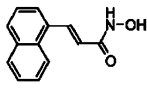
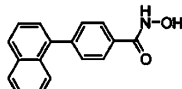
					
Ligand number	Scaffold	R	R'	IC50 HDAC1	IC50 HDAC8
7	a	C <sub>6</sub> H <sub>5</sub> CH <sub>2</sub> CH <sub>2</sub>	3,4,5-(OMe) <sub>3</sub> C <sub>6</sub> H <sub>2</sub> CH <sub>2</sub>	0.026 <sup>b</sup>	0.35 <sup>b</sup>
8	a	p-(MeO)C <sub>6</sub> H <sub>4</sub>	HOCH <sub>2</sub> CH <sub>2</sub>	4.32 <sup>b</sup>	0.40 <sup>b</sup>
9	a	C <sub>6</sub> H <sub>5</sub> CH <sub>2</sub> CH <sub>2</sub>	Me <sub>2</sub> NCH <sub>2</sub> CMe <sub>2</sub> CH <sub>2</sub>	0.024 <sup>b</sup>	0.35 <sup>b</sup>
10	a	Cyclohexyl	HOCH <sub>2</sub> CH <sub>2</sub>	3.24 <sup>b</sup>	0.20 <sup>b</sup>
11	b	(2-methylpyrrolidine-1-yl)CH <sub>2</sub>	C <sub>6</sub> H <sub>5</sub> CH <sub>2</sub>	6.30 <sup>c</sup>	0.60 <sup>c</sup>
12	b	C <sub>6</sub> H <sub>5</sub> (CH <sub>2</sub> ) <sub>2</sub> NHCH <sub>2</sub>	H	6.50 <sup>c</sup>	0.54 <sup>c</sup>
13	b	C <sub>6</sub> H <sub>5</sub> (CH <sub>2</sub> ) <sub>2</sub> NHCH <sub>2</sub>	CH <sub>3</sub>	3.50 <sup>c</sup>	0.35 <sup>c</sup>
14	b	C <sub>6</sub> H <sub>5</sub> (CH <sub>2</sub> ) <sub>2</sub> NHCH <sub>2</sub>	MeOCH <sub>2</sub> CH <sub>2</sub>	3.30 <sup>c</sup>	0.22 <sup>c</sup>
15	b	C <sub>6</sub> H <sub>5</sub> CH <sub>2</sub> NHCH <sub>2</sub>	MeOCH <sub>2</sub> CH <sub>2</sub>	3.00 <sup>c</sup>	0.13 <sup>c</sup>
16	c	H	p-(F <sub>3</sub> C)O-C <sub>6</sub> H <sub>4</sub> CH <sub>2</sub>	>1 <sup>d</sup>	<0.1 <sup>d</sup>
17	c	H	p-Cl-C <sub>6</sub> H <sub>4</sub> CH <sub>2</sub>	>10 <sup>d</sup>	<0.1 <sup>d</sup>
18	c	H	p-Me-C <sub>6</sub> H <sub>4</sub> CH <sub>2</sub>	>10 <sup>d</sup>	<0.1 <sup>d</sup>
19	c	H	(3-fluoro-4-methoxyphenyl)methyl	>10 <sup>d</sup>	<0.1 <sup>d</sup>
20	c	H	p-(F <sub>2</sub> HC)O-C <sub>6</sub> H <sub>4</sub> CH <sub>2</sub>	>10 <sup>d</sup>	<0.1 <sup>d</sup>
21	c	H	p-MeO-C <sub>6</sub> H <sub>4</sub> CH <sub>2</sub>	>10 <sup>d</sup>	<0.1 <sup>d</sup>
22	c	H	-CH=CH-CH <sub>2</sub> -phenyl	>10 <sup>d</sup>	<0.1 <sup>d</sup>
23	d	p-F-C <sub>6</sub> H <sub>4</sub> CH <sub>2</sub>	CH <sub>3</sub>	>10 <sup>d</sup>	<0.1 <sup>d</sup>

Table 5. Continued

		 			
		e	f		
Ligand number	Scaffold	R	IC50 HDAC1 <sup>a</sup>	IC50 HDAC8 <sup>a</sup>	
24	e	H	0.033 <sup>e</sup>	1.87 <sup>e</sup>	
25	e	NH <sub>2</sub>	0.099 <sup>e</sup>	2.50 <sup>e</sup>	
26	e	<sup>t</sup> BuOCONH	0.057 <sup>e</sup>	1.72 <sup>e</sup>	
27	e	NH <sub>2</sub> CH <sub>2</sub> CONH	0.10 <sup>e</sup>	3.48 <sup>e</sup>	
28	e	C <sub>6</sub> H <sub>5</sub> CH <sub>2</sub> CH(NH <sub>2</sub> )CONH	0.041 <sup>e</sup>	1.60 <sup>e</sup>	
29	e	(pyrrolidin-2-yl)CONH	0.052 <sup>e</sup>	2.66 <sup>e</sup>	
30	e	(1H-indol-3-yl)CH <sub>2</sub> CH(NH <sub>2</sub> )CONH	0.027 <sup>e</sup>	1.72 <sup>e</sup>	
31	e	p-HO-C <sub>6</sub> H <sub>4</sub> CH <sub>2</sub> CH(NH <sub>2</sub> )CONH	0.037 <sup>e</sup>	2.06 <sup>e</sup>	
32	f	H	0.003 <sup>e</sup>	1.90 <sup>e</sup>	
33	f	o-NO <sub>2</sub>	0.038 <sup>e</sup>	3.93 <sup>e</sup>	
34	f	m-NO <sub>2</sub>	0.009 <sup>e</sup>	4.09 <sup>e</sup>	
35	f	o-NH <sub>2</sub>	0.003 <sup>e</sup>	1.43 <sup>e</sup>	
36	f	m-NH <sub>2</sub>	0.004 <sup>e</sup>	1.95 <sup>e</sup>	
37	f	m-(NH <sub>2</sub> CH <sub>2</sub> CONH)	0.002 <sup>e</sup>	1.94 <sup>e</sup>	
38	f	m-(EtOCONH)	0.003 <sup>e</sup>	0.79 <sup>e</sup>	
39	f	o-( <sup>t</sup> BuOCONH)	0.012 <sup>e</sup>	1.85 <sup>e</sup>	
40	f	m-( <sup>t</sup> BuOCONH)	0.004 <sup>e</sup>	2.58 <sup>e</sup>	
41	f	m-( <sup>t</sup> BuCONH)	0.011 <sup>e</sup>	1.99 <sup>e</sup>	
42	f	m-(cyclohexylCONH)	0.002 <sup>e</sup>	3.95 <sup>e</sup>	
     					
43			>100 <sup>f</sup>	20 <sup>f</sup>	
44			>100 <sup>f</sup>	14 <sup>f</sup>	
45			-	6.6 <sup>f</sup>	
46			-	66 <sup>f</sup>	
47			>100 <sup>f</sup>	0.7 <sup>f</sup>	
48			>100 <sup>f</sup>	0.3 <sup>f</sup>	

<sup>a</sup> All activities have been determined with spectrofluorimetric methods. <sup>b</sup> Reference 25. <sup>c</sup> Reference 27. <sup>d</sup> Reference 28. <sup>e</sup> Reference 25. <sup>f</sup> Reference 29.

gram.<sup>53</sup> Most of the nonconserved residues are >5 Å away from the active site, except the ones shown in Table 6. We monitored these residues since in principle they can be involved in ligand selectivity.

The same ligands as for HDAC8 were docked into the active site of HDAC1. Again, the two oxygen atoms of the ZBG coordinate to the zinc, whose coordination sphere is saturated by Asp176, Asp264, and His178. These residues



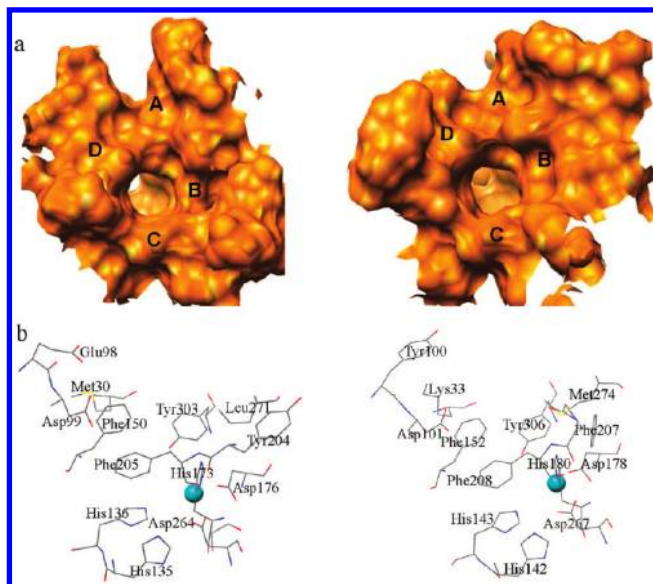


**Figure 2.** (a) Top view of the binding site surface of the HDAC1 homology model (left) and HDAC8 crystal structure with PDB code 1T69 (right). In capital letters, the main cavities of the surface are given. (b) Front view of the binding sites of HDAC1 (left) and HDAC8 (right).

correspond to HDAC8's Asp178, Asp267, and His180, respectively. The ZBG participates in hydrogen bonds with His140, His141, Asp176, His178, and Tyr303, which correspond to His142, His143, Asp178, His180, and Tyr306, respectively, in HDAC8. In the literature, two contiguous histidines, one aspartate and one tyrosine, have also been reported to form hydrogen bonds with the ZBG.<sup>58</sup> Again, all these ZBG hydrogen bonds are conserved all throughout our series of ligands.

As for the HDAC8–inhibitor complexes, the linker is always embedded in a lipophilic environment, whose walls comprise Gly149, Phe150, His178, Tyr204, and Phe205. However, the channel in HDAC1 has a wider opening as compared to HDAC8 (Figure 2), which allows for a greater ligand flexibility. The lack of Tyr100, corresponding to Glu98 in HDAC1, and the different structure of the L2 loop make the D region completely exposed to the solvent, and the presence of Leu271 in place of Met274 partially removes the border between the A and the B pockets. Additionally, the C region is larger in HDAC1 than in HDAC8 because of the lack of the Gly206 backbone. On the other hand, the B pocket of HDAC1 is narrower than in HDAC8 because of the Leu271 residue branching off. Once again, interactions with the A, B, C, or D regions of the HDAC1 surface develop within each of the studied HDAC1–inhibitor complexes.

The HDAC1 inhibitory activity trend within compounds 7–42 is quite clear: all the compounds with **a**, **b**, **c**, and **d** scaffolds display  $IC_{50}$  values  $>3 \mu M$ , while the longest **e**- and **f**-scaffolded compounds 24–42 span a nanomolar range of activities. Compounds 7 and 9 are the only exceptions, with low  $IC_{50}$  values despite the presence of a short linker.

All of the compounds bearing **b**, **c**, and **d** scaffolds place their CGs into the A region (see Figure 3), toward Tyr303. On the other hand, the aromatic or cyclic substituents belonging to the **a**-scaffolded compounds adopt different orientations. In particular, compounds 8 (cyan in Figure 3b) and 10 (green in Figure 3b) direct their rings toward the C

pocket, and their hydroxyethyl groups interact with Asp99 through a hydrogen bond. In contrast, compounds 7 (cyan in Figure 3a) and 9 (gray in Figure 3a), bearing quite bulky R and R' substituents, orient their phenylethyl moieties toward the D pocket, so benefiting from aromatic and lipophilic interactions with Phe150 and Met30 (the latter corresponding to Lys33 in HDAC8), while their R' substituents lie in the B pocket. Among all the compounds with **a**, **b**, **c**, and **d** scaffolds, only 7 and 9 explore the D pocket, so whether this region might be involved in key interactions with the protein surface will be discussed later.

Analysis of the orientations of compounds 24–42 shows that they generally prefer to make contact with the D surface, giving rise to a hydrogen bond between their amidic NH and Asp99 (see Figure 3d). In this way, their CG points toward the L2 loop, in a region delimited by Pro29, Met30, and Phe103 (corresponding to Ala32, Lys33, and Thr105 in HDAC8, respectively) as well as by Pro101. The longest compounds, such as compound 30 (gray in Figure 3d), place their biphenyl moiety inside the A pocket and direct the substituent toward the L2 loop, so orienting the terminal ring of their CG toward the same region as the other analogues. There is a slight difference between the orientations of the **f**-scaffolded thiazole derivatives and the **e**-scaffolded compounds due to the comparatively strong interaction of the heterocycle with Glu98, as evidenced by a comparison between 24 (orange) and 32 (cyan) in Figure 3d. It is hypothesized that the ion–dipole interaction involving Glu98 and the thiazole ring elicits the 10-fold higher activities of the compounds with the **f** scaffold.

For HDAC1 too, compounds 43–48 show a disposition similar to that of compounds 16–23, but their small size only allows a slight interaction with the surface, directing the aromatic CG toward region A.

In conclusion, as far as the activities of HDAC1 inhibitors are concerned, in this case too, in analogy with HDAC8, docking does not reveal a key set of residues yet highlights some peculiar regions of this isozyme, which are able to stabilize the CG better than other ones. In particular, the D pocket displays a residue arrangement poised to interact with the hydrophobic substituents of the long HDAC1-selective inhibitors.

**HDAC1/HDAC8 Selectivities.** A qualitative analysis of the HDAC8 and HDAC1 binding sites shows high similarity in the inner part of the channel but reveals some important variations due to nonconserved residues on the surface. The key interactions for HDACs inhibitor binding, apart from those involving the ZBG, appear to be the  $\pi$ – $\pi$  interactions between the central aromatic scaffold and Phe150/Phe205 (in the case of HDAC1) or Phe152/Phe208 (in the case of HDAC8), the CG orientation being crucial for selectivity.

The “T-shaped” compounds 7–15 insert their R and R' substituents into opposite pockets on the protein surface. In the case of HDAC8, the D region is too small to surround a substituent, so the bulky R and R' moieties of the comparatively low-activity compounds 7, 9, and 11 occupy the A and C pockets (Figure 3a). On the other hand, relatively small R' moieties lie toward Asp101, which typically allows the bulkier R substituent to occupy the B pocket (Figure 3b). In this region, the lipophilic portion of the inhibitors is presumably well stabilized by interactions with the Met274 and Phe207 nonconserved residues. Such hydrophobic



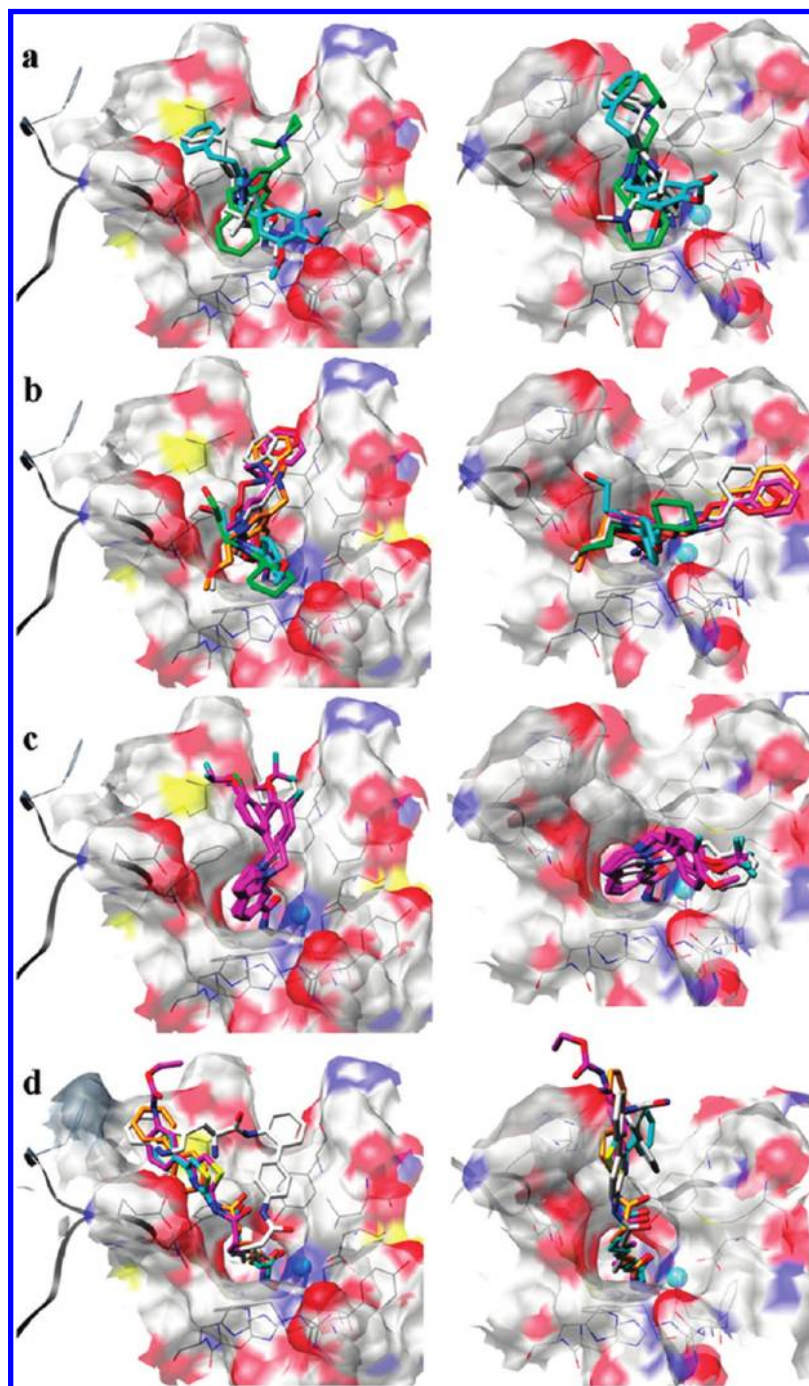


**Figure 3.** Top view of the docking orientations of the following compounds into HDAC1 (left) and HDAC8 (right): (a) **7** (cyan), **9** (gray), **11** (green); (b) **8** (cyan), **10** (green), **12** (magenta), **13** (red), **14** (orange), and **15** (gray); (c) **16–21**, **23** (magenta), **22** (gray); (d) **24** (orange), **30** (gray), **32** (cyan), **38** (magenta).

interactions cooperate with the hydrogen bonds that the hydroxyl or methoxyl R' groups of compounds **9**, **13**, and **14** establish with Asp101 to guarantee an effective stabilization of these quite active inhibitors. Further evidence of the importance of the B pocket for HDAC8 selectivity comes from the orientation of compounds **16–23**, which are the most active molecules against this enzyme. The compounds of this ligand set bear only one substituent, which lies in the B pocket of HDAC8 and interacts with it very strongly. On the other hand, in the case of HDAC1, compounds **16–23** direct their CGs toward the A region, because of the different shape and smaller size of the B pocket, as a result of the presence of Leu271 and Tyr204 in place of Met274 and Phe207, and of the lack of Gly206. Such an orientation only

allows an interaction with Tyr303 and seems not to be effective for HDAC1 activity. Indeed, HDAC1 activities are very low for these compounds.

Regarding HDAC1, its D pocket is surmised to play a similar role in CG stabilization as compared to the B pocket of HDAC8. In fact, Met30 (corresponding to Lys33 in HDAC8) can stabilize aromatic moieties in cooperation with Phe152. Among the “T-shaped” compounds **7–15**, only compounds **7** and **9** occupy the entrance of the peculiar D pocket in HDAC1 and are the most active and selective ones within this ligand set.

Finally, all of the HDAC1-selective compounds **24–42** selectively interact with the D pocket, which permits a good

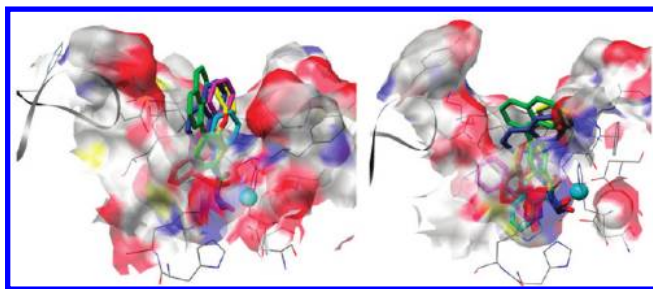


**Figure 4.** Front view of the docking orientations of compounds **43** (magenta), **44** (cyan), **45** (yellow), **46** (red), **47** (blue), and **48** (green) into HDAC1 (left) and HDAC8 (right).

**Table 6.** Nonconserved Residues Closer than 5 Å to the Active Site of HDAC1 and HDAC8

HDAC1	HDAC8
Met30	Lys33
Pro29	Ala32
Glu98	Tyr100
Leu139	Trp141
Ile177	Leu179
Glu203	Gly206
Tyr204	Phe207
Arg270	Pro273
Leu271	Met274

stabilization of their CGs in the region near the L2 loop through the Met30, Pro29, Phe103, and Pro101 residues.

In conclusion, the docking analysis seems to suggest that HDAC8/HDAC1 selectivity is principally due to the different interactions with the protein surface. In fact, aromatic or lipophilic CGs are stabilized in the B region of HDAC8 and in the D region of HDAC1. The distance between the center of the channel opening and the core of the D region in HDAC1 is about 10 Å, as compared to the 5 Å distance between the channel and the B pocket of HDAC8. This could explain the activity trend of compounds **7–48** in the two HDAC isoforms as well as suggest the starting point for designing new selective inhibitors.

**3D-QSAR Analysis.** In order to support the docking results and identify through a GRID<sup>55</sup> calculation which are the key residues for the selectivity between the two HDAC isoforms, we performed a 3D-QSAR study through the GOLPE<sup>54</sup> program on compounds **7–42** using the docking poses as receptor-based alignments for the model. The reliabilities of the 3D-QSAR models were characterized by their correlation coefficient ( $r^2$ ) and predictive correlation coefficient ( $q^2$ ), calculated using the cross-validation routine with five random sets of compounds.

Table 7 and Figure 5 report the 3D-QSAR analysis data obtained for HDAC8 and HDAC1 using the poses obtained through the SMC-ChemScore docking method as well as the C3, N2, and O probes without any fractional factorial design (FFD) calculation.

The second partial least squares (PLS) component of the HDAC8 model was able to rationalize up to 90% of variance for all the probes with a small range of  $q^2$  in between 0.76 and 0.79. The optimal dimensionality for the HDAC1 model was provided by three components, which rationalized about 93% of variance for all the probes with a worse predictive capability for the O probe ( $q^2 = 0.69$ ). The very similar predictive potential of the three probes is in agreement with the graphical model representation of the 3D-QSAR analysis,

**Table 7.** Statical Results of the 3D-QSAR Models Using C3, N2, and O Probes

	HDAC8			HDAC1		
	PC	$r^2$	$q^2$	PC	$r^2$	$q^2$
C3	2	0.921	0.775	3	0.931	0.739
N2	2	0.931	0.759	3	0.946	0.729
O	2	0.930	0.793	3	0.927	0.690

in particular with the PLS pseudocoefficient plots. These are very useful to visualize favorable and unfavorable interactions between the probes and the molecules under study when superimposed on the HDACs binding sites to highlight the activity determining regions.

In Figure 5, the positive (green polyhedrons) and negative (cyan polyhedrons) PLS coefficients for the C3, N2, and O probes are represented for HDAC8 and HDAC1. For both the enzymes, positive and negative maps corresponding to the three probes are positioned in the same regions. The main effect evidenced by the N2 and O probes in these portions of space can be considered to be of steric nature with a very low contribution arising from hydrogen-bond contacts for both HDAC1 and HDAC8.

In HDAC1 the negative a and b regions, in which a favorable interaction between a substituent and the N2 and O probes, or an unfavorable interaction between a substituent and the C3 probe results in an increase in activity, lie in the inner part of the binding site. The a region corresponds to the aromatic moiety of Tyr303 and extends beyond Leu271; the b region, on the other hand, lies near Asp99. There is only one positive region a' in which a favorable interaction between a substituent and the C3 probe or an unfavorable interaction between a substituent and the N2/O probes results in a increase of activity. This MIF is positioned in an external region of the binding site delimited by Pro29, Pro101, Phe103, and Phe150, near Met30.

In HDAC8, the MIF disposition is very different. There are two main regions (A–B) in the overlapping negative C3, N2, and O maps, where a favorable interaction between a substituent and the N2 or O probes or an unfavorable interaction with the C3 probe results in an increase in activity. The B region lies near the hydroxyl group of Tyr306. There are two corresponding positive regions (A'–B') in which a favorable interaction between a substituent and the C3 probe or an unfavorable interaction between a substituent and the N2/O probes results in a increase in activity. A' corresponds

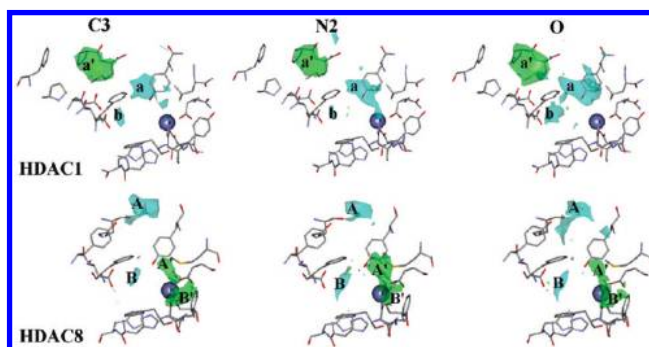


**Figure 5.** Overlap of the positive regions (green) for the C3 probe and of the negative regions (blue) for C3, N2, and O probes of the PLS coefficients plots with the HDAC1 and HDAC8 binding sites.



to Met274, while B' corresponds to Phe207, both nonconserved residues.

The MIF analysis highlights that the lipophilic interactions of the inhibitors with the D region of HDAC1 and the B region of HDAC8 are determinant for selectivity. Moreover, it reveals that the influence of Tyr303 and Asp99 is more important for HDAC1, although these residues are conserved in HDAC8.

## CONCLUSIONS

HDACs are compelling drug targets in the fight against cancer. However, isozyme selectivity, while tantalizing for clarifying the functions of the different HDACs, is still difficult to attain and far from being explained. Herein, we developed a docking protocol for HDAC1 and HDAC8. First, we analyzed the potential of the Gold program as a computational tool for predicting the binding disposition of known HDAC8 inhibitors. The optimized procedure was subsequently used to dock into HDAC1 and HDAC8 about 40 ligands that had been tested for their inhibitory activity against the two HDAC isozymes. Analysis of the best binding poses allowed us to extract qualitative information about the ligand–receptor interactions and pinpoint the ligand structural features and the protein residues important for activity and selectivity. Furthermore, the best poses were used as an alignment tool for the development of a 3D-QSAR model and for analyzing the GRID results. The results obtained allowed us to extract qualitative information about the ligand–receptor interactions.

Our findings indicate that the activities are mainly determined by hydrogen bonds established by the ZBG, polar interactions arising from Asp99/Asp101 (in HDAC1/8, respectively), aromatic stacking interactions involving Phe150/152 and Phe205/208, and various surface interactions which are peculiar to each HDAC isoform. The latter are probably determinant for HDAC8/HDAC1 selectivity and occur in a long pocket near the L2 loop of HDAC1, where Pro29, Met30, Pro101, and Phe103 can stabilize the CG, and in a region between Met274 and Phe207 in HDAC8. Also, the 3D-QSAR analysis and, in particular, superimposition of the PLS coefficient surfaces with the HDACs structures confirmed these results. The different distances between the channel opening and the B and D microdomains could be the basis of the HDAC8 selectivity exhibited by short compounds, such as **16–23** and **43–48**, and of the HDAC1 selectivity displayed by long-linker and substituted-CG compounds, such as **24–42**. Our preliminary results, albeit qualitative, can be capitalized upon toward the design of new selective HDACIs and encourage us to carry ahead further studies on other related enzymes.

## ACKNOWLEDGMENT

This article is dedicated to Dr. Francesco Di Colo, who died prematurely a few days after the redaction of this manuscript. Many thanks are due to Prof. Gabriele Cruciani and Prof. Sergio Clementi (Molecular Discovery and MIA srl) for the use of the GOLPE program in their chemometric laboratory (University of Perugia, Italy) and for having provided the GRID program.

## REFERENCES AND NOTES

- (1) Kornberg, R. D.; Lorch, Y. Twenty-five years of the nucleosome, fundamental particle of the eukaryote chromosome. *Cell* **1999**, *98*, 285–294.
- (2) Jenuwein, T.; Allis, C. D. Translating the histone code. *Science* **2001**, *293*, 1074–1080.
- (3) Peterson, C. L.; Laniel, M. A. Histones and histone modifications. *Curr. Biol.* **2004**, *14*, R546–551.
- (4) Struhl, K. Histone acetylation and transcriptional regulatory mechanism. *Gene Dev.* **1998**, *12*, 599–606.
- (5) Moggs, J. G.; Goodman, J. I.; Trosko, J. E.; Roberts, R. A. Epigenetics and cancer: implications for drug discovery and safety assessment. *Toxicol. Appl. Pharmacol.* **2004**, *196*, 422–430.
- (6) Brown, K. L.; Bren, U.; Stone, M. P.; Guengerich, F. P. Inherent stereospecificity in the reaction of aflatoxin B1 8,9-epoxide with deoxyguanosine and efficiency of DNA catalysis. *Chem. Res. Toxicol.* **2009**, *22*, 913–917.
- (7) Zhang, H.; Bren, U.; Kozekov, I. D.; Rizzo, C. J.; Stec, D. F.; Guengerich, F. P. Steric and electrostatic effects at the C2 atom substituent influence replication and miscoding of the DNA deamination product deoxyxanthosine and analogs by DNA polymerases. *J. Mol. Biol.* **2009**, *392*, 251–269.
- (8) North, B. J.; Marshall, B. L.; Borra, M. T.; Denu, J. M.; Verdin, E. The human Sir2 ortholog, SIRT2, is an NAD<sup>+</sup>-dependent tubulin deacetylase. *Mol. Cell* **2003**, *11*, 437–444.
- (9) Hubbert, C.; Guardiola, A.; Shao, R.; Kawaguchi, Y.; Ito, A.; Nixon, A.; Yoshida, M.; Wang, X.-F.; Yao, T.-P. HDAC6 is a microtubule-associated deacetylase. *Nature* **2002**, *417*, 455–458.
- (10) Holbert, M. A.; Marmorstein, R. Structure and activity of enzymes that remove histone modifications. *Curr. Opin. Struct. Biol.* **2005**, *15*, 673–680.
- (11) Marks, P. A.; Richon, V. M.; Miller, T.; Kelly, W. K. Histone deacetylase inhibitors. *Adv. Cancer Res.* **2004**, *91*, 137–168.
- (12) Somech, R.; Izraeli, S.; Amos, J. S. Histone deacetylase inhibitors—a new tool to treat cancer. *Cancer Treat. Rev.* **2004**, *30*, 461–472.
- (13) Kelly, W. K.; Richon, V. M.; O'Connor, O.; Curley, T.; MacGregor-Curtelli, B.; Tong, W.; Klang, M.; Schwartz, L.; Richardson, S.; Rosa, E.; Drobnjak, M.; Cordon-Cordo, C.; Chiao, J. H.; Rifkind, R.; Marks, P. A.; Scher, H. Phase I Clinical Trial of Histone Deacetylase Inhibitor: Suberoylanilide Hydroxamic Acid Administered Intravenously. *Clin. Cancer Res.* **2003**, *9*, 3578–3588.
- (14) Gore, S. D.; Weng, L.-J.; Zhai, S.; Figg, W. D.; Donehower, R. C.; Dover, G. J.; Grever, M.; Griffin, C. A.; Grochow, L. B.; Rowinsky, E. K.; Zabalena, Y.; Hawkins, A. L.; Burks, K.; Miller, C. B. Impact of the putative differentiating agent sodium phenylbutyrate on myelodysplastic syndromes and acute myeloid leukemia. *Clin. Cancer Res.* **2001**, *7*, 2330–2339.
- (15) Pauer, L. R.; Olivares, J.; Cunningham, C.; Williams, A.; Grove, W.; Kraker, A.; Olson, S.; Nemunaitis, J. Phase I study of oral CI-994 in combination with carboplatin and paclitaxel in the treatment of patients with advanced solid tumors. *Cancer Invest.* **2004**, *22*, 886–896.
- (16) Richards, D. A.; Boehm, K. A.; Waterhouse, D. M.; Wagener, D. J.; Krishnamurthi, S. S.; Rosemurgy, A.; Grove, W.; Macdonald, K.; Gulyas, S.; Clark, M.; Dasse, K. D. Gemcitabine plus CI-994 offers no advantage over gemcitabine alone in the treatment of patients with advanced pancreatic cancer: results of a phase II randomized, double-blind, placebo-controlled, multicenter study. *Ann. Oncol.* **2006**, *17*, 1096–1102.
- (17) Marshall, J. L.; Rizvi, N.; Kauh, J.; Dahut, W.; Figueroa, M.; Kang, M. H.; Figg, W. D.; Wainer, I.; Chaissang, C.; Li, M. Z.; Hawkins, M. J. A phase I trial of depsipeptide (FR901228) in patients with advanced cancer. *J. Exp. Ther. Oncol.* **2002**, *2*, 325–332.
- (18) Finnin, M. S.; Donigian, J. R.; Cohen, A.; Richon, V. M.; Rifkind, R. A.; Marks, P. A.; Breslow, R.; Pavletich, N. P. Structures of a histone deacetylase homologue bound to the TSA and SAHA inhibitors. *Nature* **1999**, *401*, 188–193.
- (19) Nielsen, T. K.; Hildmann, C.; Dickmanns, A.; Schwenhorst, A.; Ficner, R. J. Crystal structure of a bacterial class 2 histone deacetylase homologue. *J. Mol. Biol.* **2005**, *354*, 107–120.
- (20) Somoza, J. R.; Skene, R. J.; Katz, B. A.; Mol, C.; Ho, J. D.; Jennings, A. J.; Luong, C.; Arvai, A.; Buggy, E.; Chi, J.; Tang, B. C.; Sang, E.; Verner, R.; Wynands, E. M.; Leahy, D. R.; Dougan, G.; Snell, M.; Navre, J. J.; Knuth, M. W.; Swanson, R. V.; McRee, D. E.; Tari, L. W. Structural Snapshots of Human HDAC8 Provide Insights into the Class I Histone Deacetylases. *Structure* **2004**, *12*, 1325–1334.
- (21) Bottomley, M. J.; Lo Surdo, P.; Di Giovine, P.; Cirillo, A.; Scarpelli, R.; Ferrigno, F.; Jones, P.; Neddermann, P.; De Francesco, R.; Steinkuhler, C.; Gallinari, P.; Carfi, A. Structural and Functional Analysis of the Human Hdac4 Catalytic Domain Reveals a Regulatory Zinc-Binding Domain. *J. Biol. Chem.* **2008**, *283*, 26694–26704.
- (22) Schuetz, A.; Min, J. R.; Allali-Hassani, A.; Loppnau, P.; Kwiatkowski, N. P.; Mazitschek, R.; Edwards, A. M.; Arrowsmith, C. H.; Vedadi,

- M.; Bochkarev, A. Plotnikov, A. N. Crystal structure of the human histone deacetylase HDAC7. Manuscript in preparation.
- (23) Wang, D. F.; Helquist, P.; Wiech, N. L.; Wiest, O. Toward selective histone deacetylase inhibitor design: homology modeling, docking studies, and molecular dynamics simulations of human class I histone deacetylases. *J. Med. Chem.* **2005**, *48*, 6936–6947.
  - (24) Wu, T. Y. H.; Hassig, C.; Wu, Y.; Ding, S.; Schultz, P. G. Design, synthesis, and activity of HDAC inhibitors with a N-formyl hydroxylamine head group. *Bioorg. Med. Chem. Lett.* **2004**, *14*, 449–453.
  - (25) Kozikowski, A. P.; Chen, Y.; Gaysin, A. M.; Savoy, D. N.; Billadeau, D. D.; Kim, K. H. Chemistry, biology, and QSAR studies of substituted biaryl hydroxamates and mercaptoacetamides as HDAC inhibitors: nanomolar-potency inhibitors of pancreatic cancer cell growth. *ChemMedChem* **2008**, *3*, 487–501.
  - (26) Chen, D.; Deng, W.; Sangthongpitak, K.; Song, H. Y.; Sun, E. T.; Yu, N.; Zou, Y. Benzimidazole derivatives: preparation and pharmaceutical application. WO Patent 2005/028447, Mar 31, 2005.
  - (27) Deng, W.; Chen, D.; Zhou, Y. Bicyclic heterocycles: preparation and pharmaceutical application. WO Patent 2006/101456, Sep 28, 2006.
  - (28) Buggy, J. J.; Balasubramanian, S.; Verner, E.; Tai, V. W.-F.; Lee, C.-S. Indole derivatives as inhibitors of histone deacetylase. WO Patent 2007/109178, Sep 27, 2007.
  - (29) KrennHrubeck, K.; Marshall, B. L.; Hedglin, M.; Verdin, E.; Ulrich, S. M. Design and Evaluation of 'Linkerless' hydroxamic acids as selective HDAC8 inhibitors. *Bioorg. Med. Chem. Lett.* **2007**, *17*, 2874–2878.
  - (30) Sternson, S. M.; Wong, J. C.; Grozinger, C. M.; Schreiber, S. L. Synthesis of 7200 small molecules based on a substructural analysis of the histone deacetylase inhibitors trichostatin and trapoxin. *Org. Lett.* **2001**, *3*, 4239–4242.
  - (31) Haggarty, S. J.; Koeller, K. M.; Wong, J. C.; Grozinger, C. M.; Schreiber, S. L. Domain-selective small-molecule inhibitor of histone deacetylase 6 (HDAC6)-mediated tubulin deacetylation. *Proc. Natl. Acad. Sci. U.S.A.* **2003**, *100*, 4389–4394.
  - (32) Hu, E.; Dul, E.; Sung, C.-M.; Chen, Z.; Kirkpatrick, R.; Zhang, G.-F.; Johanson, K.; Liu, R.; Lago, A.; Hofmann, G.; Macarron, R.; De Los Frailes, M.; Perez, P.; Krawiec, J.; Winkler, J.; Jaye, M. Identification of Novel Isoform-Selective Inhibitors within Class I Histone Deacetylases. *J. Pharmacol. Exp. Ther.* **2003**, *307*, 720–728.
  - (33) Waltregny, D.; De Leval, L.; Glenisson, W.; Ly Tran, S.; North, B. J.; Bellahcene, A.; Weidle, U.; Verdin, E.; Castronovo, V. Expression of Histone Deacetylase 8, a Class I Histone Deacetylase, Is Restricted to Cells Showing Smooth Muscle Differentiation in Normal Human Tissues. *Am. J. Pathol.* **2004**, *165*, 553–564.
  - (34) Waltregny, D.; Glenisson, W.; Tran, S. L.; North, B. J.; Verdin, E.; Colige, A.; Castronovo, V. Histone deacetylase HDAC8 associates with smooth muscle-actin and is essential for smooth muscle cell contractility. *FASEB J.* **2005**, *19*, 966–968.
  - (35) Durst, K. L.; Lutterbach, B.; Kummalue, T.; Friedman, A. D.; Hiebert, S. W. The inv(16) Fusion Protein Associates with Corepressors via a Smooth Muscle Myosin Heavy-Chain Domain. *Mol. Cell. Biol.* **2003**, *23*, 607–619.
  - (36) Kishimoto, M.; Kohno, T.; Okudela, K.; Otsuka, A.; Saski, H.; Tanabe, C.; Sakiyama, T.; Hirama, C.; Kitabayashi, I.; Minna, J. D.; Takenoshita, S.; Yokota, J. Mutations and deletions of the CBP gene in human lung cancer. *Clin. Cancer Res.* **2005**, *11*, 512–519.
  - (37) Ishihama, K.; Yamakawa, M.; Semba, S.; Takeda, H.; Kawata, S.; Kimura, S.; Kimura, W. Expression of HDAC1 and CBP/p300 in human colorectal carcinomas. *J. Clin. Pathol.* **2007**, *60*, 1205–1210.
  - (38) Zhu, P.; Martin, E.; Mengwasser, J.; Schlag, P.; Janssen, K.-P.; Göttlicher, M. Induction of HDAC2 expression upon loss of APC in colorectal tumorigenesis. *Cancer Cell* **2004**, *5*, 455–463.
  - (39) Senese, S.; Zaragoza, K.; Minardi, S.; Muradore, I.; Ronzoni, S.; Passafaro, A.; Bernard, L.; Draetta, G. F.; Alcalay, M.; Seiser, C.; Chiocca, S. Role for Histone Deacetylase 1 in Human Tumor Cell Proliferation. *Mol. Cell. Biol.* **2007**, *27*, 4784–4795.
  - (40) Roperio, S.; Fraga, M. F.; Ballestar, E.; Hamelin, R.; Yamamoto, H.; Boix-Chornet, M.; Caballero, R.; Alaminos, M.; Setien, F.; Paz, M. F.; Herranz, M.; Palacios, J.; Arango, D.; Orntoft, T. F.; Aaltonen, L. A.; Schwartz, Jr. S.; Esteller, M. A truncating mutation of HDAC2 in human cancers confers resistance to histone deacetylase inhibition. *Nat. Genet.* **2006**, *38*, 566–569.
  - (41) Vannini, A.; Volpari, C.; Filocamo, G.; Casavola, E. C.; Brunetti, M.; Renzoni, R.; Chakravarty, P.; Paolini, C.; De Francesco, R.; Gallinari, P.; Steinkuhler, C.; Di Marco, S. Crystal structure of a eukaryotic zinc-dependent histone deacetylase, human HDAC8, complexed with a hydroxamic acid inhibitor. *Proc. Natl. Acad. Sci. U.S.A.* **2004**, *101*, 15064–15069.
  - (42) Vannini, A.; Volpari, C.; Gallinari, P.; Jones, P.; Mattu, M.; Carfi, A.; De Francesco, R.; Steinkuhler, C.; Di Marco, S. Substrate binding to histone deacetylases as shown by the crystal structure of the HDAC8-substrate complex. *EMBO Rep.* **2007**, *8*, 879–884.
  - (43) Dowling, D. P.; Gantt, S. L.; Gattis, S. G.; Fierke, C. A.; Christianson, D. W. Structural studies of human histone deacetylase 8 and its site-specific variants complexed with substrate and inhibitors. *Biochemistry* **2008**, *47*, 13554–13563.
  - (44) Berman, H. M.; Westbrook, J.; Feng, Z.; Gilliland, G.; Bhat, T. N.; Weissig, H.; Shindyalov, I. N.; Bourne, P. E. The Protein Data Bank. *Nucleic Acids Res.* **2000**, *28*, 235–242.
  - (45) Maestro, ver. 7.5; Schrödinger Inc.: Portland, OR, 1999.
  - (46) MacroModel, ver. 8.5; Schrödinger Inc.: Portland, OR, 1999.
  - (47) Morris, G. M.; Goodsell, D. S.; Halliday, R. S.; Huey, R.; Hart, W. E.; Belew, R. K.; Olson, A. J. Automated docking using a Lamarckian genetic algorithm and an empirical binding free energy function. *J. Comput. Chem.* **1998**, *19*, 1639–1662.
  - (48) Jones, G.; Willett, P.; Glen, R. C.; Leach, A. R.; Taylor, R. J. Development and validation of a genetic algorithm for flexible docking. *J. Mol. Biol.* **1997**, *267*, 727–748.
  - (49) Huang, C. C.; Couch, G. S.; Pettersen, E. F.; Ferrin, T. E. The object technology framework: an object-oriented interface to molecular data and its application to collagen. *Pac. Symp. Biocomput.* **1996**, *1*, 724; <http://www.cgl.ucsf.edu/chimera>.
  - (50) Soeding, J. Protein homology detection by HMM-HMM comparison. *Bioinformatics* **2005**, *21*, 951–960.
  - (51) Hughey, R.; Krogh, A. Hidden Markov models for sequence analysis: Extension and analysis of the basic method. *Computer Appl. Biosci.* **1996**, *12*, 95–107.
  - (52) Altschul, S. F.; Madden, T. L.; Schäffer, A. A.; Zhang, J.; Zhang, Z.; Miller, W.; Lipman, D. Gapped BLAST and PSI-BLAST: a new generation of protein database search programs. *Nucleic Acid Res.* **1997**, *25*, 3389–3402.
  - (53) Fiser, A.; Do, R. K.; Sali, A. Modeling of loops in protein structures. *Protein Sci.* **2000**, *9*, 1753.
  - (54) GOLPE, Version 4.5; Multivariate Infometric Analysis Srl.: Perugia, Italy, 1999.
  - (55) GRID, Version 22a; Molecular Discovery Ltd.: West Way House, Elms Parade, Oxford, U.K., 2004.
  - (56) Estiu, G.; Greenberg, E.; Harrison, C. B.; Kwiatkowski, N. P.; Mazitschek, R.; Bradner, J. E.; Wiest, O. Structural origin of selectivity in class II-selective histone deacetylase inhibitors. *J. Med. Chem.* **2008**, *51*, 2898–2906.
  - (57) Tuccinardi, T.; Nuti, E.; Ortore, G.; Rossello, A.; Avramova, S. I.; Martinelli, A. Development of a receptor-based 3D-QSAR study for the analysis of MMP2, MMP3, and MMP9 inhibitors. *Bioorg. Med. Chem. Lett.* **2008**, *16*, 7749–7758.
  - (58) Ragno, R.; Mai, A.; Massa, S.; Cerbara, I.; Valente, S.; Bottoni, P.; Scatena, R.; Jesacher, F.; Loidl, P.; Brosch, G. 3-(4-Aroyl-1-methyl-1H-pyrrol-2-yl)-N-hydroxy-2-propenamides as a New Class of Synthetic Histone Deacetylase Inhibitors. 3. Discovery of Novel Lead Compounds through Structure-Based Drug Design and Docking Studies. *J. Med. Chem.* **2004**, *47*, 1351–1359.
  - (59) Heltweg, B.; Dequiedt, F.; Marshall, B. L.; Brauch, C.; Yoshida, M.; Nishino, N.; Verdin, E.; Jung, M. Subtype selective substrates for histone deacetylases. *J. Med. Chem.* **2004**, *47*, 5235–5243.
  - (60) Blackwell, L.; Norris, J.; Suto, M. C.; Janzen, W. P. The use of diversity profiling to characterize chemical modulators of the histone deacetylases. *Life Sci.* **2008**, *82*, 1050–1058.